The electrode-electrolyte interface in CO2 reduction and H2 evolution: a multiscale approach

Cecilio de Oliveira Monteiro, M

2

Measuring local pH in electrochemistry

This chapter is based on: Monteiro, M. C. O., Koper, M. T. M. *Current Opinion in Electrochemistry, 25,* 100649 (2020)

Abstract

Localized pH measurements are important in various areas of electrochemistry, from corrosion to bio-electrochemistry and electrocatalysis. Different techniques are available to perform these measurements and offer numerous possibilities in terms of spatial and temporal resolution, sensitivity, and precision. In this brief review we present the recent progress made and summarize the main techniques available for localized pH measurements in electrochemistry such as scanning probe techniques (SECM, SICM, SIET), laser (confocal) fluorescence microscopy, rotating ring-disc electrode (RRDE) voltammetry, and infra-red spectroscopy, among others.

2.1 Introduction

The concept of pH as we know it today dates back to 1909 when Sørensen introduced the pH scale as a way to express the concentration of hydrogen ions.[1] In electrochemistry, the local concentration of protons in solution plays a significant role in reactions of different fields and is a function of the substrate geometry, the current density, mass transport, and the buffer capacity of the electrolyte. Corrosion via anodic oxidation is usually associated with metal dissolution and hydrolysis, thus locally producing protons.[2] Various biological processes cause intra- or extracellular pH changes and the quantification of these pH changes can help to understand the associated mechanisms.[3] Numerous electrocatalytic processes such as O_2 evolution or CO_2 reduction, that consume or produce H^+ or OH^-, generate a pH gradient between the working electrode (substrate) and the bulk of the electrolyte.[4] In all these applications, measuring the pH locally and with high sensitivity is desired to better understand the electrochemical processes involved.

Shortly after the invention of the glass pH electrode, scientists started putting efforts towards its miniaturization to perform what one could consider the first localized pH measurement ever reported: pH of arterial blood flowing through a small cannula in the cortex of a monkey.[5] It was already concluded at that time, that producing miniaturized pH probes “is quite possible, with practice”. Since then, electrochemists have invested significant efforts to develop not only new probes but also new techniques to measure pH locally with high spatial and temporal resolution. Here, we give an overview of those developments, together with a brief discussion of their advantages, drawbacks, and applicability. The techniques can be divided into direct and indirect methods to measure pH, namely techniques in which the signal monitored is the proton concentration by measuring its electrochemical potential (scanning probe microscopy, rotating ring-disc electrode) or techniques that probe species, whose signal is a function of the proton concentration (fluorescence and infrared intensities). Localized pH measurements can help to elucidate reaction mechanisms and assist in the deconvolution of pH effects from other electrolyte or structural surface effects. The rate at which the pH changes can also help understanding the stability of a certain substrate, to probe mass transport phenomena or reactivity. Spatial resolution, temporal resolution, and sensitivity will dictate which of these system properties can be captured by the different methods.

2.2 Scanning probe techniques: SECM, SICM, and SIET

Scanning probe microscopy (SPM) techniques used for pH measurements usually consist of monitoring the electrochemical signal of a miniaturized tip (ultramicroelectrode or nanoelectrode) while the tip is moved above a substrate. High spatial resolution can be achieved in three dimensions (XYZ) and is limited by the size and geometry of the tip, taking into account the radial diffusion profile towards ultramicroelectrodes (UMEs). The spatial resolution can be improved and the shielding can be minimized by miniaturizing the pH sensor and the insulating layer around it. Temporal resolution, precision, selectivity, and stability, on the other hand, are highly dependent on the nature of the pH sensor. In the next sections we discuss the main SPM techniques used to probe pH locally in electrochemistry, namely: Scanning Electrochemical Microscopy (SECM), Scanning Ion-selective Electrode Technique (SIET) and Scanning Ion Conductance Microscopy (SICM).

2.2.1 SECM

Among the different SPM techniques, SECM is the most employed to probe local pH. Normally, the tip is made of an inert or metallic material with a pH-sensitive electrochemical response, surrounded by an insulator. A schematic representation of an SECM setup is shown in Fig. 2.1a. Local pH measurements have been performed using either potentiometric or voltammetric sensors. Potentiometric pH probes consist of substrates whose open circuit potential shows a Nernstian (59 mV/pH) or super-Nernstian (> 59 mV/pH) shift as a function of pH. They are mainly based on metals, metal/metal oxides (TiO_2, RuO_2, RhO_2, Ta_2O_5, IrO_2, PtO_2, and ZrO_2)[6] or electrodeposited polymer films.[7] Among these, IrO_2 is the most popular substrate. Tefashe et al. used a Pt/IrO_2 probe to measure pH during localized corrosion of AZ31B magnesium alloy electrochemically coated with poly(3,4-ethylenedioxythiophene) (PEDOT).[8] The pH map obtained after 30 min immersion in 0.01 M NaCl can be seen in Fig. 2.1b, recorded with the pH probe positioned 10 μm from the surface. Other metal supports can also be used, as seen in the work of Santos and co-workers[9], where pH above a copper surface during nitrate reduction was measured with a Au/IrO_2 probe. Polymer films have also been used as potentiometric sensors. The most popular is polyaniline (PANI) due to its high conductivity and ease of synthesis. Recently Song et al. reported the use of a PANI coated Pt ultramicroelectrode to monitor the extracellular pH of MCF-7 cells

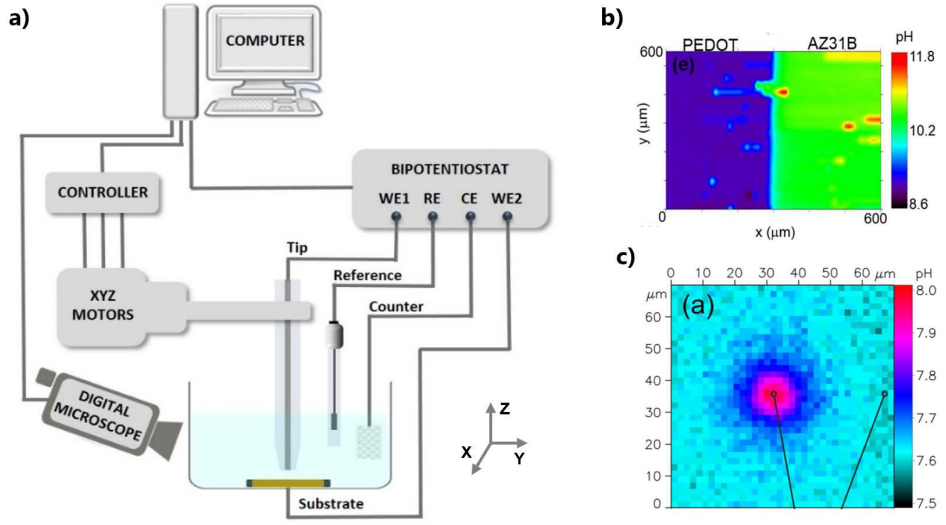

Fig. 2.1. a) Schematic representation of a scanning probe setup, **b)** pH map of uncoated and PEDOT-coated AZ31B Mg alloy after 30 min in 0.01 M NaCl, measured with a Pt/IrOx microprobe operated in constant height potentiometric mode of SECM. Adapted from Ref. 8. **c)** pH map during oxygen reduction on a 10 μm diameter Pt disc recorded with a voltammetric pH nanosensor made of a syringaldazine polymeric film. Adapted with permission from Ref. 15. Copyright (2015) American Chemical Society.

under electrical stimulation.[10] The main advantage of potentiometric pH sensors, in general, is their easy manufacturing, which facilitates their miniaturization. However, the fact that the pH response comes from the interaction of protons in solution with a solid-state film, means that potentiometric pH sensors have a relatively long response time of usually a few seconds, which can change as a function of pH.[11] The overall performance is also highly affected by the quality and thickness of the film. The synthesis of potentiometric pH sensors usually does not involve complicated steps and is often done via electrodeposition. Although there is an extensive list of synthesis protocols reported in literature[12], the success rate, even when following a well-established recipe, is known to be low. Potential drift can also prevent direct pH determination from the initial calibration curve and often requires recalibration.[13] Besides, the potential gradient across the interface being studied can potentially affect the open circuit potential recorded at the tip. The mentioned drawbacks can lead to strong deviations in the measurements (especially when pH maps are being constructed) and require a systematic data processing protocol.

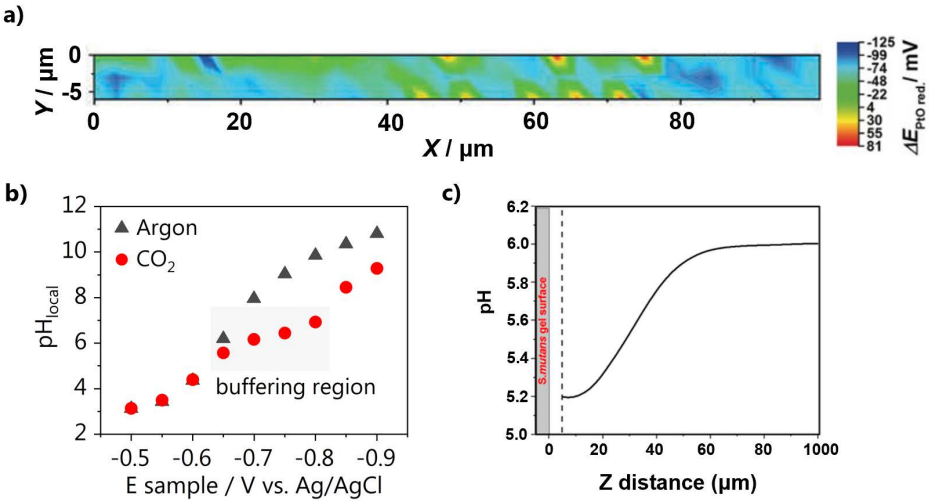

Fig. 2.2. a) Image of the shifts in the reduction peak potential of a Pt nanoelectrode during oxygen reduction at a Ag-based gas diffusion electrode. Each grid point was measured at 1 µm tip-surface distance utilizing shear force constant distance mode SECM. Adapted with permission from Ref. 14. Copyright (2018) Wiley-VCH Verlag GmbH & Co. KGaA. **b)** Buffering effect during CO_2 reduction measured with a voltammetric pH sensor based on a gold UME functionalized with a 4-NTP self-assembled monolayer (Chapter 4). **c)** Z-directional pH profile recorded with a glass capillary filled with an ion-selective cocktail, from 50 µm above the S. mutans biofilm to 1000 µm in the bulk solution after addition of 30 mM sucrose in artificial saliva (pH 6.0). Adapted with permission from Ref. 23. Copyright (2017) American Chemical Society.

Alternatively, SECM voltammetric pH sensors can be employed. They are based on the current-potential response of a certain redox reaction (upon cycling) and the pH is determined by the Nernstian shift of the reduction or oxidation midpeak potential. Voltammetric probes have the major advantage that the response time is only dependent on the time required to record a cyclic voltammogram and can easily be tuned. Michalak et al. have probed pH during ORR using a voltammetric pH nanosensor based on a syringaldazine film. The pH map obtained above a Pt-UME is shown in Fig. 2.1c.[14] The same type of sensor was also successfully applied to monitor the extracellular pH of adherently growing mammalian cells.[15] As syringaldazine is electropolymerized on a substrate, the influence of film thickness and stability on the pH response is still a concern. Botz et al. used the PtO reduction voltammetry to also successfully probe pH during oxygen reduction (ORR) over a silver gas diffusion electrode as can be seen in Fig.

2.2a.[16] Although a Pt-UME is suitable to probe the high alkalinity developed during ORR, unfortunately, it cannot be easily applied to other systems, as the Pt response is not exclusively selective to pH. We have recently presented a pH sensor that overcomes film and selectivity limitations, based on a self-assembled monolayer of 4-nitrothiophenol (4-NTP) on a Au-UME (Chapter 3 of this thesis).[17] The sensor is extremely sensitive, capturing differences as small as 0.1 pH units and is stable and selective in diverse electrolytes and under different gaseous atmospheres. This enables, for instance, pH measurements during CO_2 reduction on gold using SECM, as shown in Fig. 2.2b (Chapter 4 of this thesis).[61] We have recently also successfully employed our Au-UME/4-NTP pH sensor to better understand CO bulk electrooxidation in the CO_2 reduction reaction environment, through combined SECM measurements (Chapter 5 of this thesis).[18]

For mapping pH with high resolution above a substrate, pH sensors must be positioned accurately in solution at a controlled distance from the surface of interest. Commonly used SECM approach techniques need a mediator or a diffusion-limited reaction taking place at the tip to determine the tip-to-sample distance. However, not all pH sensors allow for diffusion-controlled feedback, as not always current can be drawn without destabilizing the tip response. The development of double-barrelled UMEs or dual probes overcomes positioning issues allowing for diffusion-controlled feedback, using the amperometric side of the tip, while carrying out pH measurements with the other side.[19,20] Other (more refined) distance control feedback systems employ shear-force[21], introduced by the group of Schuhmann, or alternating current-SECM (AC-SECM)[22]. We have also recently presented the application of a capacitive approach, performed in air, to determine the tip-to-surface distance without destabilizing the pH sensor.[17] The intricacies and applicability of commonly used distance control methods are well discussed in the book of Bard and Mirkin.[23]

2.2.2 Scanning Ion-selective Electrode (SIET)

SIET is a technique very similar to SECM, albeit employing potentiometric pH sensors that consist of a liquid ion-selective membrane enclosed in a (pulled) micro- or nanopipette. Different proton selective cocktails have been reported and many are commercially available (Fluka, Selectophore®). Joshi et al. reported the use of a H^+ selective cocktail to map the pH of the microenvironment produced by the lactate-producing S. mutans biofilm. Fig. 2.2c shows a profile in Z-direction of the pH monitored 950 µm across the diffusion layer.[24] The dynamic pH range of

these probes is usually limited so they are mostly used for measurements in the physiologically relevant pH range, or in corrosion processes where the pH changes are not too drastic.[25–27] The main drawbacks here are similar to those discussed for the potentiometric SECM probes, i.e. slow time response (limiting the scanning speed that can be used when imaging pH), fouling, and damage to the ion-selective electrode. Additionally, manufacturing requires expertise. New fabrication procedures have been reported to improve the response time by decreasing the electrode resistance. However, to date, no pH measurements have been reported with these improved probes.[28]

2.2.3 Scanning Ion Conductance Microscopy (SICM)

SICM is another powerful technique that has been used to perform pH measurements. In standard SICM, the scanning probe is a pulled nanopipette that is filled with an electrolyte containing a quasi-reference counter electrode (e.g. Ag/AgCl). Distance control is obtained by applying a potential between the tip and an external quasi-reference counter electrode placed in the bulk electrolyte which generates an ionic conductance current (feedback signal). To perform pH measurements with SICM, double-barrel SICM-SECM pipettes are used, which allow for simultaneously controlling the position of the electrode with high spatial resolution and measuring the pH locally.

A schematic representation of a SICM experimental setup is shown in Fig. 2.3a. Here, a zwitterionic label-free nanoprobe was combined with SICM in a double-barrelled nanopipette to probe the topography and pH of single living cancer cells, with 50 nm spatial resolution.[29] Fig. 2.3b shows the simultaneously obtained fluorescence image, SICM topography, and pH distribution of a group of low-buffered breast cancer MCF7 cells in an estradiol-deprived medium. Despite the remarkable results, the zwitterionic pH probe response is only linear in a narrow pH range between 5 and 8, making it mainly applicable to biological systems. Other (more robust) pH sensing substrates, on the other hand, allow for pH measurements in a wider pH range. Nadappuram et al.[30] used nanoscale double-barrelled pipettes with IrO_2 for pH measurements and a SICM barrel for distance control. The probe was used to map the topography and pH of a calcite microcrystal. The maps obtained with a 10 μm lateral resolution can be seen in Fig. 2.3c, where they are compared to an optical image of the microcrystal. Polymeric pH sensors have also been used in combination with SICM, as reported in the work of Morris et al.[31], who

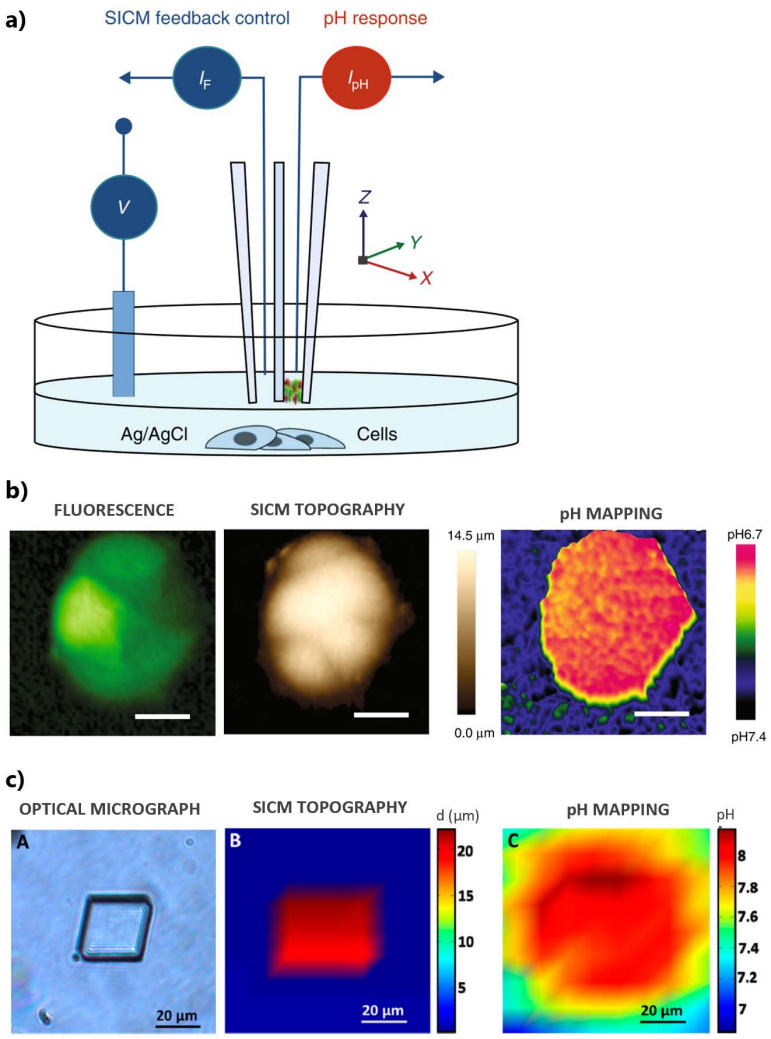

Fig. 2.3. a) Schematic representation of the operation of double-barrel nanopipettes for simultaneous SICM imaging and pH measurement and **b)** fluorescence and SICM imaging of a group of low-buffered $CD44^{GFP\text{-}high}$ breast cancer MCF7 cells in estradiol-deprived medium (−E2), together with a high resolution pH map, all simultaneously obtained from a single scan. Adapted from Ref. 28. **c)** Optical micrograph of a calcite microcrystal compared to a simultaneously recorded SICM topography image and pH map measured 100 nm from the microcrystal (bulk pH 6.85). Adapted with permission from Ref. 29. Copyright (2013) American Chemical Society.

used a Au/PANi barrel to measure pH in porous membranes. While SECM pH probes are employed with or without positional feedback (depending on the probe´s size and the nature of the substrate), positioning control is intrinsic of SICM, which makes it, combined with other techniques as SECM and fluorescence, a powerful tool for obtaining detailed information of the electrochemical interface. Similar to SIET, fabrication of the probes requires expertise.

2.3 Rotating Ring-Disc Electrode

Measuring pH under well-defined mass transport conditions using a Rotating Ring-Disc Electrode (RRDE) system was introduced by Albery and Calvo[32] and since then mainly employed to probe electrocatalytic reactions. The operation principle is similar to SECM in the sense that an electrode is used to measure pH. In the RRDE system, a shaft is connected to a rotator and the cross-section of the shaft contains two working electrodes, a disc electrode surrounded by a thin ring electrode. The ring is used to probe the flux of species coming from the disc with a certain collection (or detection, depending on the pH sensor used) efficiency that will depend on the electrode´s dimensions (radius, spacing). Initially, mainly bare Pt was used as ring material, however, that limits the number of systems that can be investigated as Pt is not a very selective H^+ sensor. In later work, the ring was modified with a potentiometric pH sensing layer, as IrO_2, which allows the use of the technique to probe a larger variety of systems, as shown in Fig. 2.4a. With the electrode shown in Fig. 2.4a, Zimer et al.[33] investigated the influence of rotation rate on the steady-state water reduction on copper. Results from Fig. 2.4b show the pH measured by the ring as a function of the rotation rate and indicate that a steady-state is achieved at rotation rates over 1200 rpm. RRDE has been employed to study other reactions as hydrogen oxidation[34], CO_2 reduction[35], oxygen reduction[36], and ethanol oxidation.[37] Additionally, it has also been used to probe electrodeposition processes, as nickel electrodeposition.[38] The main advantage of using a RRDE is that it is one of the few techniques that allows for the measurement of pH under defined mass transport conditions. On the other hand, the measurements are not spatially resolved in XY (as it probes the flux of species coming from the whole disc surface). The resolution in Z is limited and is a function of the rotation speed. It can be obtained by modelling of the system. Additionally, the time resolution to fully capture the process taking place at the disc is dependent on the time response of the pH sensor used. In Chapter 6 of this thesis, we show the application of the pH

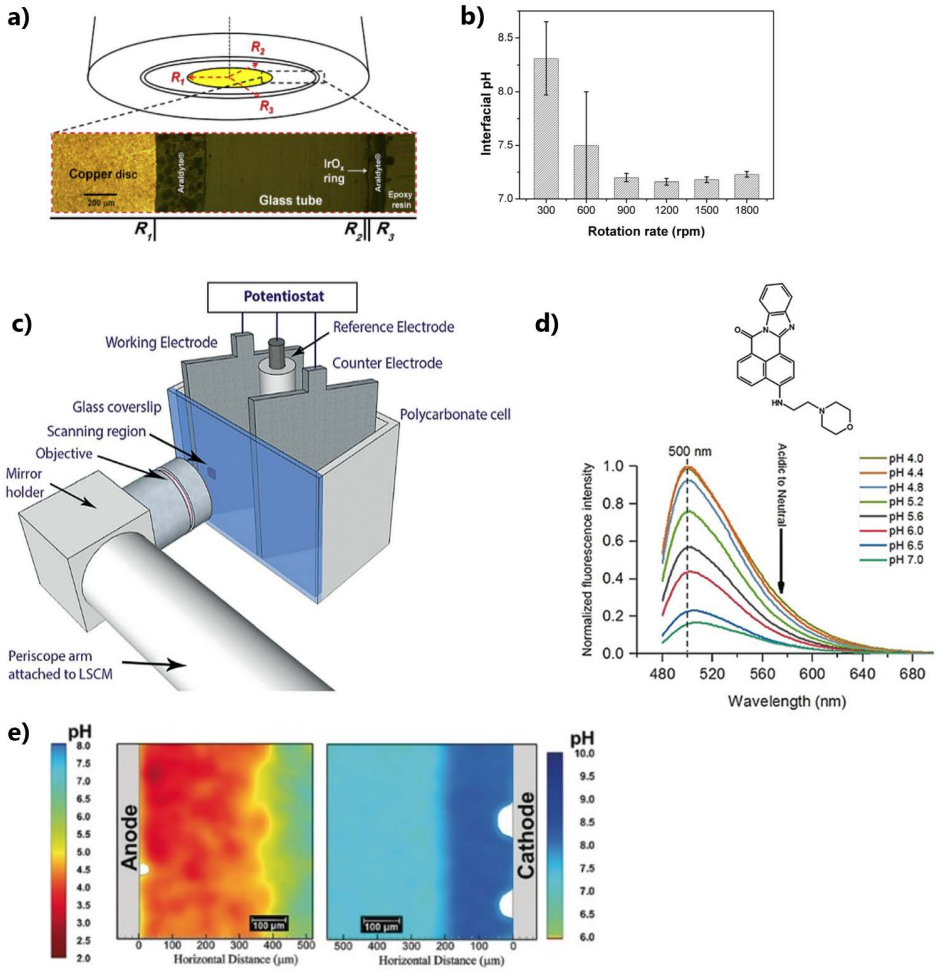

Fig. 2.4. a) Schematic representation of an RRDE pH sensor and **b)** measurements performed with it during water reduction on copper at different rotation rates. Adapted with permission from Ref. 32. Copyright (2015 Elsevier B.V. **c)** Schematic representation of a single compartment electrochemical cell coupled with a laser scanning confocal microscope, **d)** chemical structure of the LysoSensor Green DND-189 dye together with its normalized fluorescence response in phosphate buffer from pH 4 to 7, **e)** pH distribution at the anode and cathode during electrocoagulation, after a current density of 2 mA cm^{-2} is applied for 60 s. Figures c, d and e are adapted from Ref. 46. Copyright (2019) Wiley VCH Verlag GmbH & Co. KGaA.

sensor developed in Chapter 3 to RRDE, allowing for measurements with high sensitivity and temporal resolution.

2.4 Optical techniques

Various methods can be used to probe proton concentration gradients locally by using the optical properties of (electro)generated or consumed species, fluorescence being the most popular. In general, the measured optical property can be absorption or fluorescence intensity, decay time, reflectance, refractive index, light scattering, or light polarization.[39] We have selected fluorescence, infrared and Raman spectroscopy to briefly discuss here.

2.4.1 Fluorescence microscopy

Fluorescence has been widely used to indirectly measure pH in electrochemical systems. The most employed strategy is to add a pH-sensitive fluorophore to the electrolyte. The protons or OH^- produced/consumed by an electrochemical process can modulate the signal of the species in solution, which is captured using a fluorescence microscope. The workable pH range is determined by the pK_a of the fluorophores used. It is a versatile technique, that can be adapted to numerous electrochemical systems. The classic wide-field illumination setup allows for in situ mappings of pH in X- and Y-directions.[40,41] Although it has been used to record 2D pH images of different electrochemical systems, its well-known major drawback is the large signal contribution of out-of-focus light. The use of confocal laser scanning microscopy (CLSM) can overcome that by using a spatial pinhole to eliminate the out-of-focus light contribution to the image formation. It allows for mapping pH in 3D, by stacking 2D images acquired sequentially at different positions on the Z-axis. Pioneer contributions were made by the group of Unwin, demonstrating that 3D fluorescence maps can provide quantitative imaging of pH profiles during water reduction on Pt-UMEs.[42,43] CLSM has been successfully applied to measure pH in the fields of bioelectrochemistry[44,45], electrosynthesis[46], electrocatalysis[47,48], and the development of new dyes for expanding the workable pH range and stability can broaden its use even more.[49] Recently, the work of Fuladpanjeh-Hojaghan et al.[48] presented an electrochemical cell coupled with a laser scanning confocal microscope able to perform quantitative pH mapping under operando conditions during electrocoagulation (Fig. 2.4c). Two aluminium plates are used as cathode and anode and a combination of pH-sensitive fluorescent dyes with different pK_a allows for pH detection in a range from 1.5 to 8.5. An example of

the dye response upon a change in pH is shown in Fig. 2.4d for the LysoSensor Green DND-189 (LSG, pK_a 5.2). pH maps under operando conditions were obtained from the cathode and anode side and an example is shown in Fig. 2.4e, which is an image taken after 60 seconds of polarization. The anodic reaction causes aluminium dissolution and consequently aluminium cation hydrolysis, leading to acidification near the electrode surface. On the cathode side, the water reduction reaction generates a more alkaline pH near the surface. A setup for performing time-resolved CLSM pH measurements has also been recently introduced by Pande et al.[50] Fluorescein was used as a pH-sensitive fluorophore, to study the diffusion layer during ORR on platinum and the effect of sulfate buffering on the pH profiles. The results of a time-dependent numerical model give good agreement with the experimental data.

One of the main advantages of CLSM is that, differently from SPM techniques, it enables one to probe an entire macroscopic sample in real-time with high spatial resolution. Although pH maps can be obtained relatively quickly, the need of adding a fluorophore to the electrolyte is a drawback as it may affect the electrochemical process being studied. In general, the resolution limit of pH measurements using fluorescence falls into the diffraction limit of conventional light microscopes (~250 nm, considering the wavelength of green light and a numerical aperture of 1), unless a super-resolution microscopy technique is used, e.g. Stimulated Emission Depletion (STED), where pH measurements in a living cell have been performed with a resolution down to 20 nm.[51] This and other super-resolution techniques have been mainly used to probe biological substrates. Their application to other electrochemical systems is not straightforward and sometimes not possible due to the lack of stability of the pH sensing molecules.

2.4.2 Other optical techniques

pH measurements at the electrochemical interface during CO_2 reduction have recently been reported using surface-enhanced infrared absorption spectroscopy (SEIRAS).[52–54] The signal intensity of species that compose a buffer system, such as CO_2/HCO_3^- or $H_2PO_4^-/HPO_4^{2-}/PO_4^{3-}$, is monitored. Using the equilibrium equations, the average proton concentration at the interface can be indirectly derived from the ratio of the signal of these species. Valuable information can be obtained regarding the species in solution only a few nanometers from the electrode surface in the Z direction, averaged over a large portion of the surface in XY. These measurements do not provide spatial resolution and require IR active

Table 2.1. Overview of techniques discussed in this work to measure local pH in electrochemistry

Technique	pH sensor	pH range	Application	Type	Reference
SECM					
Potentiometric	IrOx/Au	2-11	Nitrate reduction	direct	9
	IrOx/Pt	1-13	Corrosion of 316L stainless steel, Corrosion of AZ31B Magnesium Alloy	direct	8,55,56
	Sb/Sb_2O_3	4-11	Corrosion of AZ63 magnesium alloy	direct	19
	Polyaniline/ Pt	4-8	extracellular pH	direct	10
	Pt	1-8	Methanol oxidation, enzymatic processes	direct	57
Voltammetric	syringaldazine	2-12	Oxygen reduction, extracellular pH	direct	15,16
	4-NTP monolayer on Au	1-12	Hydrogen evolution, CO_2 reduction on gold	direct	17 (Chapter 3), 61 (Chapter 4), 18 (Chapter 5)
SICM	zwitterion nano-membrane	4-9	Extracellular pH	direct	28
	IrOx/C	2-10	Dissolution of a calcite microcrystal	direct	29
	Polyaniline/Au	2.5-12	Nano channels of a membrane	direct	30
SIET	H^+-selective cocktail	4-10	Microbial metabolism	direct	23
	Hydrogen ionophore I - cocktail B (Selectophore™)	5-12.5	Corrosion of MA8 Mg alloy	direct	26
FLUORESCENCE	LSG + 5(6)-carboxynaphtho-fluorescein	1.5-8.5	Electrocoagulation	indirect	46
	fluorescein	5.5-7	H_2O and O_2 reduction, enzymatic O_2 reduction, coaxial flow micro-reactor	indirect	41,43,44
RRDE	Pt	5-9	H_2 evolution and oxidation	direct	33
	IrO_2	2.5-12.5	H_2O reduction	direct	32
	Pt, IrO_2	n.a.	CO_2 reduction on gold	direct	34
INFRARED	$H_2PO_4^-/HPO_4^{2-}/PO_4^{3-}$	5-13	CO_2 reduction on copper	indirect	52
	CO_2/ HCO^{3-}	n.a.	CO_2 reduction on gold	indirect	50
RAMAN	4-mercaptobenzoic acid/Au nanoparticle	2-12	Aerosol microdroplets	indirect	54

species in the electrolyte. Similarly to the dyes used in fluorescence, the pK_a of these species in equilibrium will dictate the pH range that can be measured. Raman Spectroscopy has also been used to probe pH.[55] Wei et al. developed pH nanoprobes based on plasmonic gold nanoparticles functionalized with a pH-sensitive amine or carboxylic acid. The nanoprobes were used to detect the intracellular pH of PC-3 cancer cells[56] and the pH gradients within phosphate-buffered aerosol microdroplets with a lateral resolution of 5 µm.[57] The technique is powerful to investigate micro-environments, however, can only be applied to specific systems where the addition of the signal enhancing pH-sensitive particles is feasible. Differently than in SPM, the resolution that can be achieved in pH measurements performed with optical techniques is defined by the operating system and not by the size of the pH probe.

2.5 Final considerations

Having discussed the main techniques that can be used to measure pH in electrochemistry, we have grouped a few examples in Table 2.1 to provide a general overview of the methods available, the pH range that can be measured, and the kind of systems that can be investigated with each technique. To conclude, we highlight the following:

- The main advantages of SPM for performing localized pH measurements are the high spatial resolution in X-Y-Z that can be achieved, and the versatility in terms of the sample, probes, and modes available, to be chosen according to the application. A wide pH range can be studied with a series of established potentiometric and voltammetric sensors. Voltammetric sensors are especially interesting, due to the high temporal resolution that can be achieved. The main disadvantage of SPM is shielding caused by the probe.[58] However, this can be significantly minimized by the use of nanopipettes. Additionally, these contributions can be simulated and accounted for with finite element models.
- Optical methods have the great advantage of being non-invasive techniques, and the use of a confocal laser microscope allows for achieving spatial resolutions comparable to SPM techniques. However, altering the electrolyte composition by the addition of a fluorophore is a major drawback. Additionally, the operational pH range is usually limited by the pK_a of the pH-sensitive species.

- Infrared and Raman spectroscopy can be powerful tools to probe small volumes of the electrochemical interface, although the spatial resolution in Z cannot be tuned and the XY resolution is limited by the beam size.
- Combining SPM and optical techniques can be highly effective to obtain detailed information about complex electrochemical systems, see e.g. SECM-SICM[30], SECM-fluorescence[59], SECM-infrared.[60]
- RRDE pH measurements are especially interesting for mechanistic studies as the defined mass transport control of the system allows for a more precise modeling of the reaction interface. On the other hand, the measurements are not spatially resolved and represent an average response of the whole working electrode.

There has been intensive development of methods for measuring pH in electrochemistry lately. Knowing precisely the research questions that need answers is key for defining the most suitable technique to investigate a given system. We believe the combined knowledge obtained through the different techniques discussed here, can enable a deeper understanding of complex electrochemical systems.

References

(1) Sörensen, S. P. L. *Ergebnisse der Physiol.* 1909, 21, 131–200.
(2) Jadhav, N.; Gelling, V. J. *J. Electrochem. Soc.* 2019, *166* (11), C3461–C3476.
(3) Orij, R.; Brul, S.; Smits, G. J. *Biochim. Biophys. Acta - Gen. Subj.* 2011, *1810* (10), 933–944.
(4) Ooka, H.; Figueiredo, M. C.; Koper, M. T. M. *Langmuir* 2017, *33* (37), 9307–9313.
(5) Nims, L. F. *Yale J. Biol. Med.* 1938, *10* (3), 241–246.
(6) Manjakkal, L.; Szwagierczak, D.; Dahiya, R. *Prog. Mater. Sci.* 2020, *109*, 100635.
(7) Korostynska, O.; Arshak, K.; Gill, E.; Arshak, A. *Sensors* 2007, *7* (12), 3027–3042.
(8) Tefashe, U. M.; Dauphin-Ducharme, P.; Danaie, M.; Cano, Z. P.; Kish, J. R.; Botton, G. A.; Mauzeroll, J. *J. Electrochem. Soc.* 2015, *162* (10), C536–C544.
(9) Santos, C. S.; Lima, A. S.; Battistel, D.; Daniele, S.; Bertotti, M. *Electroanalysis* 2016, *28* (7), 1441–1447.
(10) Song, R.; Xiong, Q.; Wu, T.; Ning, X.; Zhang, F.; Wang, Q.; He, P. *Anal. Bioanal. Chem.* 2020, *412* (15), 3737–3743.
(11) Zhang, X.; Ogorevc, B.; Wang, J. *Anal. Chim. Acta* 2002, *452* (1), 1–10.
(12) Jang, H.; Lee, J. *J. Energy Chem.* 2020, *46*, 152–172.
(13) Etienne, M.; Dierkes, P.; Erichsen, T.; Schuhmann, W.; Fritsch, I. *Electroanalysis* 2007, *19* (2), 318–323.
(14) Michalak, M.; Kurel, M.; Jedraszko, J.; Toczydlowska, D.; Wittstock, G.; Opallo, M.; Nogala, W. *Anal. Chem.* 2015, *87* (23), 11641–11645.
(15) Munteanu, R.-E.; Stănică, L.; Gheorghiu, M.; Gáspár, S. *Anal. Chem.* 2018, *90* (11), 6899–6905.
(16) Botz, A.; Clausmeyer, J.; Öhl, D.; Tarnev, T.; Franzen, D.; Turek, T.; Schuhmann, W. *Angew. Chemie - Int. Ed.* 2018, *57* (38), 12285–12289.
(17) Monteiro, M. C. O.; Jacobse, L.; Touzalin, T.; Koper, M. T. M. *Anal. Chem.* 2020, *92* (2), 2237–2243.
(18) Monteiro, M. C. O.; Jacobse, L.; Koper, M. T. M. *J. Phys. Chem. Lett.* 2020, *11* (22), 9708–9713.
(19) Zhu, Z.; Ye, Z.; Zhang, Q.; Zhang, J.; Cao, F. *Electrochem. commun.* 2018, *88*, 47–51.
(20) Filotás, D.; Fernández-Pérez, B. M.; Nagy, L.; Nagy, G.; Souto, R. M. *Sensors Actuators, B Chem.* 2019, *296*, 126625.
(21) Ballesteros Katemann, B.; Schulte, A.; Schuhmann, W. *Chem. - A Eur. J.* 2003, *9* (9), 2025–2033.
(22) Eckhard, K.; Schuhmann, W. *Analyst* 2008, *133* (11), 1486–1497.
(23) Bard, A. J.; Mirkin, M. V. Second.; Bard, A. J., Mirkin, M. V., Eds.; CRC Press, 2012.
(24) Joshi, V. S.; Sheet, P. S.; Cullin, N.; Kreth, J.; Koley, D. *Anal. Chem.* 2017, *89* (20), 11044–11052.
(25) Lamaka, S. V.; Taryba, M.; Montemor, M. F.; Isaacs, H. S.; Ferreira, M. G. S. *Electrochem. commun.* 2011, *13* (1), 20–23.
(26) Oltra, R. *Corros. Eng. Sci. Technol.* 2018, *53*, 2–8.
(27) Gnedenkov, A. S.; Mei, D.; Lamaka, S. V.; Sinebryukhov, S. L.; Mashtalyar, D. V.; Vyaliy, I. E.; Zheludkevich, M. L.; Gnedenkov, S. V. *Corros. Sci.* 2020, *170*, 108689.
(28) Varga, Á.; Nagy, L.; Izquierdo, J.; Bitter, I.; Souto, R. M.; Nagy, G. *Anal. Lett.* 2011, *44*

(18), 2876–2886.
(29) Zhang, Y.; Takahashi, Y.; Hong, S. P.; Liu, F.; Bednarska, J.; Goff, P. S.; Novak, P.; Shevchuk, A.; Gopal, S.; Barozzi, I.; Magnani, L.; Sakai, H.; Suguru, Y.; Fujii, T.; Erofeev, A.; Gorelkin, P.; Majouga, A.; Weiss, D. J.; Edwards, C.; Ivanov, A. P.; Klenerman, D.; Sviderskaya, E. V.; Edel, J. B.; Korchev, Y. *Nat. Commun.* 2019, *10* (1), 1–9.
(30) Nadappuram, B. P.; McKelvey, K.; Al Botros, R.; Colburn, A. W.; Unwin, P. R. *Anal. Chem.* 2013, *85* (17), 8070–8074.
(31) Morris, C. A.; Chen, C. C.; Ito, T.; Baker, L. A. *J. Electrochem. Soc.* 2013, *160* (8), H430–H435.
(32) Albery, W. J.; Calvo, E. J. *J. Chem. Soc. Faraday Trans. 1 Phys. Chem. Condens. Phases* 1983, *79* (11), 2583–2596.
(33) Zimer, A. M.; Medina da Silva, M.; Machado, E. G.; Varela, H.; Mascaro, L. H.; Pereira, E. C. *Anal. Chim. Acta* 2015, *897*, 17–23.
(34) Yokoyama, Y.; Miyazaki, K.; Miyahara, Y.; Fukutsuka, T.; Abe, T. *ChemElectroChem* 2019, 4750–4756.
(35) Zhang, F.; Co, A. C. *Angew. Chemie - Int. Ed.* 2020, *59* (4), 1674–1681.
(36) Steegstra, P.; Ahlberg, E. *J. Electroanal. Chem.* 2012, *685* , 1–7.
(37) Figueiredo, M. C.; Arán-Ais, R. M.; Climent, V.; Kallio, T.; Feliu, J. M. *ChemElectroChem* 2015, *2* (9), 1254–1258.
(38) Ji, J.; Cooper, W. C.; Dreisinger, D. B.; Peters, E. *J. Appl. Electrochem.* 1995, *25* (7).
(39) Wencel, D.; Abel, T.; McDonagh, C. *Anal. Chem.* 2014, *86* (1), 15–29.
(40) Bowyer, W. J.; Xie, J.; Engstrom, R. C. *Anal. Chem.* 1996, *68* (13), 2005–2009.
(41) O´Brien, C.; Shumaker Parry, J.; Engstrom, R. C. *Anal. Chem.* 1998, *70* (7), 1307–1308.
(42) Cannan, S.; Douglas Macklam, I.; Unwin, P. R. *Electrochem. commun.* 2002, *4* (11), 886–892.
(43) Rudd, N. C.; Cannan, S.; Bitziou, E.; Ciani, I.; Whitworth, A. L.; Unwin, P. R. *Anal. Chem.* 2005, *77* (19), 6205–6217.
(44) Hou, J. T.; Ren, W. X.; Li, K.; Seo, J.; Sharma, A.; Yu, X. Q.; Kim, J. S. *Chem. Soc. Rev.* 2017, *46* (8), 2076–2090.
(45) Tassy, B.; Dauphin, A. L.; Man, H. M.; Le Guenno, H.; Lojou, E.; Bouffier, L.; De Poulpiquet, A. *Anal. Chem.* 2020, *92* (10), 7249–7256.
(46) Abou-Hassan, A.; Dufrêchfer, J. F.; Sandre, O.; Mériguet, G.; Bernard, O.; Cabuil, V. *J. Phys. Chem. C* 2009, *113* (42), 18097–18105.
(47) Leenheer, A. J.; Atwater, H. A. *J. Electrochem. Soc.* 2012, *159* (9), H752–H757.
(48) Fuladpanjeh-Hojaghan, B.; Elsutohy, M. M.; Kabanov, V.; Heyne, B.; Trifkovic, M.; Roberts, E. P. L. *Angew. Chemie Int. Ed.* 2019, *58* (47), 16815–16819.
(49) Bigdeli, A.; Ghasemi, F.; Abbasi-Moayed, S.; Shahrajabian, M.; Fahimi-Kashani, N.; Jafarinejad, S.; Farahmand Nejad, M. A.; Hormozi-Nezhad, M. R. *Anal. Chim. Acta* 2019, *1079*, 30–58.
(50) Pande, N.; Chandrasekar, S. K.; Lohse, D.; Mul, G.; Wood, J. A.; Mei, B. T.; Krug, D. *J. Phys. Chem. Lett.* 2020, *11* (17), 7042–7048.
(51) Richardson, D. S.; Gregor, C.; Winter, F. R.; Urban, N. T.; Sahl, S. J.; Willig, K. I.; Hell, S. W. *Nat. Commun.* 2017, *8* (1), 577.
(52) Ayemoba, O.; Cuesta, A. *ACS Appl. Mater. Interfaces* 2017, *9* (33), 27377–27382.
(53) Zhou, J.; Ma, H. *Chem. Sci.* 2016, *7* (10), 6309–6315.
(54) Yang, K.; Kas, R.; Smith, W. A. *J. Am. Chem. Soc.* 2019, *141* (40), 15891–15900.
(55) Zhang, Z.; Melo, L.; Jansonius, R. P.; Habibzadeh, F.; Grant, E. R.; Berlinguette, C. P.

ACS Energy Lett. 2020, *5* (10), 3101–3107.

(56) Wei, H.; Willner, M. R.; Marr, L. C.; Vikesland, P. J. *Analyst* 2016, *141* (17), 5159–5169.

(57) Wei, H.; Vejerano, E. P.; Leng, W.; Huang, Q.; Willner, M. R.; Marr, L. C.; Vikesland, P. J. *Proc. Natl. Acad. Sci. U. S. A.* 2018, *115* (28), 7272–7277.

(58) Critelli, R. A. J.; Bertotti, M.; Torresi, R. M. *Electrochim. Acta* 2018, *292*, 511–521.

(59) Boldt, F. M.; Heinze, J.; Diez, M.; Petersen, J.; Börsch, M. *Anal. Chem.* 2004, *76* (13), 3473–3481.

(60) Wang, L.; Kowalik, J.; Mizaikoff, B.; Kranz, C. *Anal. Chem.* 2010, *82* (8), 3139–3145.

(61) Monteiro, M. C. O.; Mirabal, A.; Jacobse, L.; Doblhoff-Dier, K.; Barton, S. C.; Koper, M. T. M. *JACS Au.* 2021, 1 (11), 1915–1924.